Preprints.org

Article

Not peer-reviewed version

Zinc Oxide Loaded Cellulose-based Carbon Gas Sensor for Selective Detection of Ammonia

Hao Xu , Zhu-Xiang Gong , Li-Zhu Huo , Chaofei Guo , Xue-Juan Yang , Yu-Xuan Wang * , Xi-Ping Luo *

Posted Date: 14 November 2023

doi: 10.20944/preprints202311.0857.v1

Keywords: Gas sensor; ammonia; zinc oxide; microcrystalline cellulose

Preprints.org is a free multidiscipline platform providing preprint service that is dedicated to making early versions of research outputs permanently available and citable. Preprints posted at Preprints.org appear in Web of Science, Crossref, Google Scholar, Scilit, Europe PMC.

Copyright: This is an open access article distributed under the Creative Commons Attribution License which permits unrestricted use, distribution, and reproduction in any medium, provided the original work is properly cited.

Preprints (www.preprints.org) | NOT PEER-REVIEWED | Posted: 14 November 2023 doi:10.20944/preprints202311.0857.v1

Disclaimer/Publisher's Note: The statements, opinions, and data contained in all publications are solely those of the individual author(s) and contributor(s) and not of MDPI and/or the editor(s). MDPI and/or the editor(s) disclaim responsibility for any injury to people or property resulting from any ideas, methods, instructions, or products referred to in the content.

Article

Zinc Oxide Loaded Cellulose-Based Carbon Gas Sensor for Selective Detection of Ammonia

Hao Xu, Zhu-Xiang Gong, Li-Zhu Huo, Chaofei Guo, Xue-Juan Yang, Yu-Xuan Wang * and Xi-Ping Luo *

College of Chemistry and Materials Engineering, Zhejiang A&F University, Hangzhou, Zhejiang Province 311300, PR China; jasonxu@stu.zafu.edu.cn (H.X.); 1974353023@qq.com (Z.-X.G.); 2298017026@qq.com (L.-Z.H.); chaoguo@zafu.edu.cn (C.G.); yangxuejuan2008@126.com (X.-J.Y.)

* Correspondence: 20190050@zafu.edu.cn (Y.-X.W.); luoxiping@zafu.edu.cn (X.-P.L.); Tel.: +86-131-2238-0892(Y.-X.W.); Tel.: +86-159-6888-2838 (X.-P.L.)

Abstract: Cellulose-based carbon (CBC) has been widely concerned with its porous structure, high specific surface area, and is liable to adsorb gas molecules and macromolecular pollutants. However, the application of CBC in gas sensing has been little studied. In this paper, ZnO/CBC heterojunction was formed by means of simple co-precipitation and high temperature carbonization. As a new ammonia sensor, the prepared ZnO/CBC sensor can detect ammonia compared with that of the previous pure ZnO ammonia sensor can not at room temperature. It has great gas sensing response, stability and selectivity to ammonia concentration at 200 ppm. This study provides a new idea for the design and synthesis of biomass carbon-metal oxide composites.

Keywords: Gas sensor; ammonia; zinc oxide; microcrystalline cellulose

1. Introduction

Ammonia is a colorless, toxic, corrosive substance with a strong odor and a choking effect. Excess ammonia can pose a huge threat to human health and to cause environment pollution. Different from other toxic gases, ammonia has a low boiling point of -33.5 ℃, a low melting point of -77.75 ℃, a low density of 0.771 g·L^{-1}, a refractive index of 1.33, and a dipole moment of 1.42 d. These characteristics make ammonia an excellent gas sensor, and its sensors can be used in a variety of applications such as environmental monitoring, agriculture or medical diagnostics, and industrial waste dealing [1,2].

Zinc oxide is a metal oxide semiconductor material with wide band gap (3.37 eV), high bonding strength and large exciton binding energy (60 meV) at room temperature. Based on these properties, it is often used in gas sensors, chemical sensors, biosensors, cosmetics, energy storage, optical and electronic devices and other products [3–7]. The existing zinc oxide gas sensors show great gas sensing performance for carbon dioxide, ammonia and ethanol. The resistive gas sensor based on ZnO nanosheets was prepared by Srinivasulu et al. which has a large surface area and can quickly and highly detect carbon dioxide in the air [8]. The ZnO nanoflowers were prepared by Yu et al. which have great gas sensing properties for low concentrations of ammonia [9]. However, the original zinc oxide still has some shortcomings such as poor gas sensitivity, slow response and recovery time and poor selectivity. Therefore, many researchers have used by doping other elements or mixing zinc oxide with other metal oxides to prepare composite materials in order to improving gas sensing performance [10–14].

It is an effective way to improve the gas sensing performance of the sensor by introducing carbon material into the gas sensing material based on zinc oxide. Using activated carbon fiber as a template, Chao et al. synthesized ZnO/C nanoporous fibers by hydrothermal method. The materials showed great gas sensing performance to low concentrations of ethanol and acetone at optimum operating temperature [15]. The heterojunction ZnO/hollow porous carbon microtubule (CMT) prepared by Sun et al. from simple carbonized buttonwood fluff fibers showed a great gas sensing response to

© 2023 by the author(s). Distributed under a Creative Commons CC BY license.

Preprints (www.preprints.org) | NOT PEER-REVIEWED | Posted: 14 November 2023 doi:10.20944/preprints202311.0857.v1

trace ammonia molecules [16]. Hu et al. prepared composite materials by generating zinc oxide particles on nitrogen-doped carbon sheets, and the heterogeneous structure improved the gas sensing ability of composite materials to ppb grade NO_2 [17]. Cellulose, as a natural polymer material abundant on the earth, has a large number of hydroxyl functional group, excellent biodegradability and stable physical and chemical properties [18]. And compared with other carbon sources, cellulose is more available in nature, which can reduce the cost of producing carbon materials significantly. In recent years, there have been many reports on the application of cellulose-based carbon (CBC) as carbon materials in the field of supercapacitors and photocatalytic degradation by taking advantage of its excellent properties such as porous structure, huge specific surface area, and ability to adsorb gas molecules and macromolecular pollutants [19–23]. However, there are few researches on carbonizing cellulose into biomass carbon materials into ZnO-based gas sensors.

In this work, zinc oxide was prepared by a simple chemical precipitation method, and then it was carbonized with microcrystalline cellulose at high temperature, and ZnO/CBC were prepared for ammonia detection. Compared with the original ZnO-based ammonia sensor, due to the construction of the heterogeneous structure between ZnO and CBC, the composite has a great gas sensing response to a certain concentration of ammonia at room temperature, and has a better ammonia selectivity. The use of cellulose as the precursor of biomass carbon materials and combined with metal oxides to form composite materials provides a new reference in the field of gas detection.

2. Materials and Methods

2.1. Materials

Zinc acetate dihydrate ($Zn(CH_3COO)_2{\cdot}2H_2O$, 98%) was get from Anneji (Shanghai) Pharmaceutical Chemical Co., Ltd. Ammonia liquor ($NH_3{\cdot}H_2O$, 26%-28%) was purchased from Sinopharm Chemical Reagent Co., Ltd. Microcrystalline cellulose (50 μm) was obtained from Aladdin Reagent (Shanghai) Co., Ltd. Deionized water was prepared in the laboratory.

2.2. Synthesis of ZnO/CBC

ZnO was prepared by a simple chemical deposition method. Add 0.25 g zinc acetate dihydrate and 0.5 g microcrystalline cellulose to 30 mL deionized water, add ammonia water under magnetic stirring in an oil bath at 90 °C, make the molar ratio of Zn^{2+} to OH^- 1:15. Continued magnetically stirring at 90 ℃ for 1h. After the reaction, the solution was washed and centrifuged for several times until the pH was neutral, and then dried in a vacuum drying oven at 60 °C to obtain a white powder. The white powder was placed in a tube furnace at 600 °C and calcined by N_2 for 2 hours. The black powder obtained was recorded as ZnO/CBC-60% (the ratio of zinc acetate dihydrate to microcrystalline cellulose). According to the same experimental methods, ZnO/CBC-33%, ZnO/CBC-50%, ZnO/CBC-66%, ZnO/CBC-71% and CBC with different zinc oxide contents were prepared.

2.3. Characterization

The morphology and size of the samples were characterized by field emission scanning electron microscopy (SEM, ZEISS Sigma 300) and transmission electron microscopy (TEM, FEI Tecnai F30). The crystal structure of the sample was characterized by X-ray diffraction (XRD, Bruker D2 PHASER) of copper target radiation at ambient temperatures with 2θ values of 10 to 80 degrees and scanning rates of 5°/mins. The chemical composition and elements of the samples were characterized by X-ray photoelectron spectroscopy (XPS, Thermo Scientific K-Alpha). Raman spectra were recorded using a Raman spectrometer (Raman, Horiba LabRAM HR Evolution) with a laser wavelength of 532 nm. In situ DRIFT spectroscopy was performed using Bruker VERTEX 80v infrared spectrometer. ZnO/CBC-60% was exposed to ammonia and pure nitrogen at room temperature. The Mott-Schottky curves of the samples were measured with an electrochemical workstation (CHI660E model), 0.5 M sodium sulfate solution is configured, Ag/AgCl is the reference electrode, platinum plate is the counter electrode.

Preprints (www.preprints.org) | NOT PEER-REVIEWED | Posted: 14 November 2023 doi:10.20944/preprints202311.0857.v1

2.4. Fabrication of gas sensing device

In order to perform electrical and sensing performance, a certain amount of samples were taken on an agate mortar and a small amount of deionized water was added to grind the samples to a sticky state. The grinding liquid was evenly coated on the interdigital electrode of the ceramic substrate and dried in a drying oven at 100 ℃. Gas sensing measurements are carried out using the self-made device shown in Figure 1. The static liquid-gas distribution method is used to generate ammonia gas environments with different concentrations. The calculation formula is shown as follows [24,25]:

$$C = \frac{22.4 \times \emptyset \times \rho \times p \times V_1}{M \times V_2} \times 1000 \quad (1)$$

where C (ppm) stand for target gas concentration, Ø stand for required gas volume fraction, ϱ (g mL $^{-1}$) stand for density of the liquid, p stand for purity of the liquid, V_1 (μL) stand for volume of liquid, V_2 (L) stand for volume of the chamber, and M (g mol^{-1}) stand for molecular weight of the liquid.

The change in resistance of the sensor was measured by a multimeter. The response of the sensor was defined as:

$$S = \frac{R_g - R_a}{R_a} \times 100\% \quad (2)$$

where R_a is the resistance of the sensor in the air, and R_g is the resistance of the sensor after it passes into the target gas.

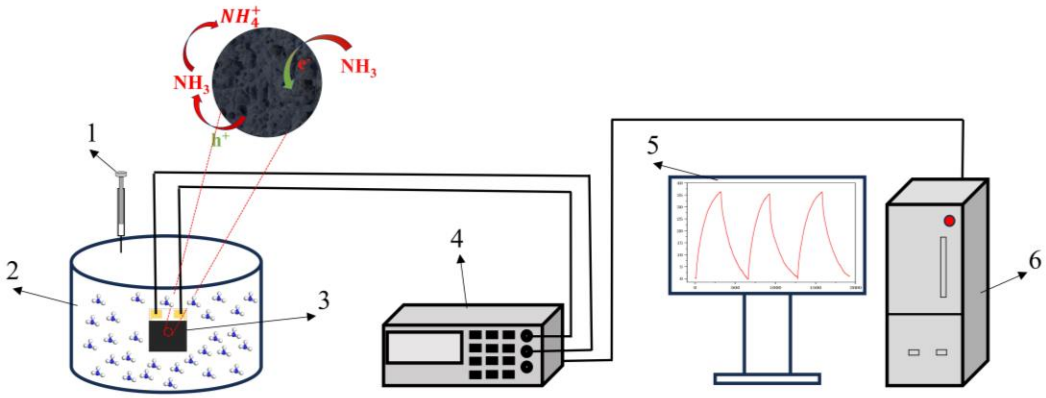

Figure 1. Schematic diagram of gas detection. (1) Syringe, (2) Reaction chamber, (3) Interdigital electrode, (4) Victor 8145C TRMS digit multimeter, (5) Display screen, (6) Mainframe computer.

3. Results

3.1. Characterization of ZnO/CBC

The XRD patterns of ZnO/CBC and CBC with different ZnO precursor contents are shown in Figure 2. ZnO/CBC showed sharp diffraction peaks at 2θ = 31.8°, 34.4°, 36.3°, 47.5°, 56.6°, 62.9°, 66.4°, 67.9°, 69.1°, 72.6° and 77.0°, which were in accordance with (100), (002), (101), (102), (110), (103), (200), (112), (201), (004) and (202) crystal planes, respectively, The strongest peak occurred on the (101) crystal plane. All diffraction peaks correspond to the standard hexagonal wurtzite structure (JCPDS-99-0111) [26,27]. No diffraction peaks from other phases or impurities were observed. These results indicated that pure ZnO structures were formed through precipitation. Since the amorphous carbon was prepared and its crystallinity is low, wide peaks with low signal strength appeared near 22 ° and 42 ° [28–30]. The diffraction peaked strength is weaker than ZnO, while there could not be shown in the XRD pattern of ZnO/CBC.

Preprints (www.preprints.org) | NOT PEER-REVIEWED | Posted: 14 November 2023 doi:10.20944/preprints202311.0857.v1

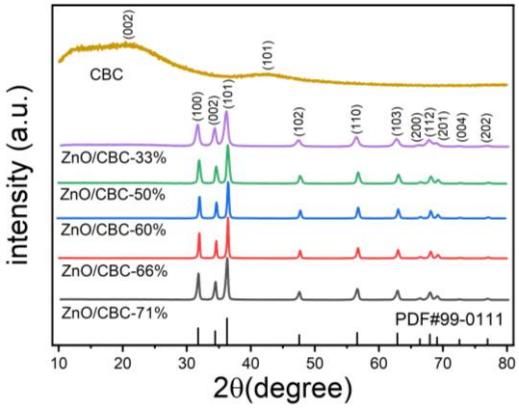

Figure 2. XRD patterns of ZnO/CBC with different ZnO contents and CBC.

Figure 3 shows the SEM images of ZnO/CBC and pure carbon with different ZnO precursor contents. It can be seen from Figure 3b–e that ZnO has been successfully loaded on CBC. ZnO exhibited a flower-like structure when the precursor content was small. With the ZnO precursor content increasing, ZnO gradually changed into a rod-like structure, at mean while the aspect ratio also becoming larger. This was due to the increase in ammonia solution, which promoted oxidation. Zinc preferentially grew on the C axis [31]. Figure 3a shows that the surface of CBC was relatively smooth after high temperature carbonization. However, after loading ZnO, the surface of CBC becomes rough. EDS was used to conduct elemental analysis of ZnO/CBC-60%. It can be seen from Figure S1 that C, O and Zn have been evenly distributed on ZnO/CBC-60%, and the atomic ratios of C, O and Zn were 77.50%, 11.84% and 10.66%, respectively. Since aluminum foil was used as the substrate, the Al signal appeared.

In order to further understood the structure of ZnO/CBC-60%, TEM characterization was performed. As shown in Figure 4a,b, it can be clearly found that there were different lattice fringes at the boundary of CBC and ZnO. The lattice fringes near 0.136 and 0.282 nm correspond to the (201) and (100) crystal faces of ZnO, respectively [11,32]. The lattice fringes near 0.202 and 0.350 nm correspond to the (101) and (002) crystal faces of graphite, respectively [33]. The lattice fringes of ZnO and CBC were interwoven, which also confirmed the construction of heterojunctions between ZnO and CBC.

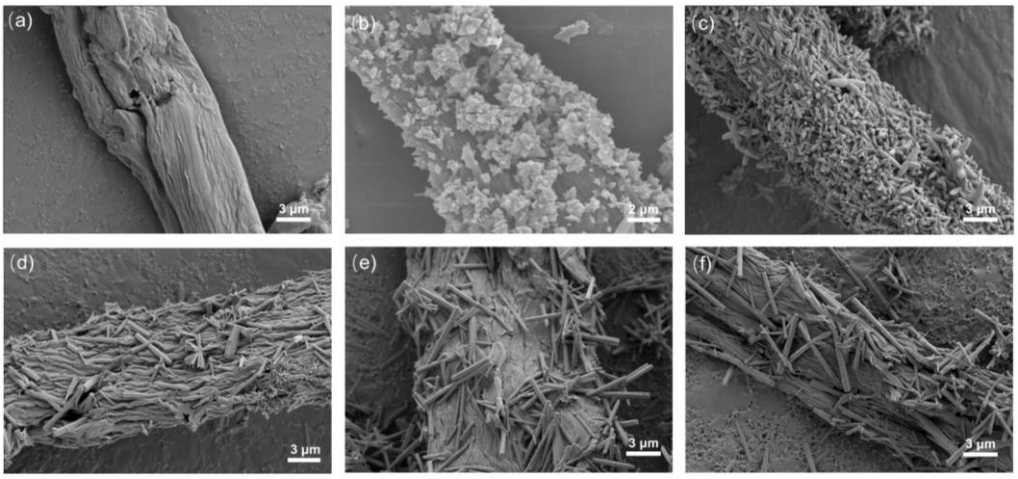

Figure 3. SEM image of (a)CBC, (b)ZnO/CBC-33%, (c)ZnO/CBC-50%, (d)ZnO/CBC-60%, (e)ZnO/CBC-66%, (f) ZnO/CBC-71%.

Preprints (www.preprints.org) | NOT PEER-REVIEWED | Posted: 14 November 2023 doi:10.20944/preprints202311.0857.v1

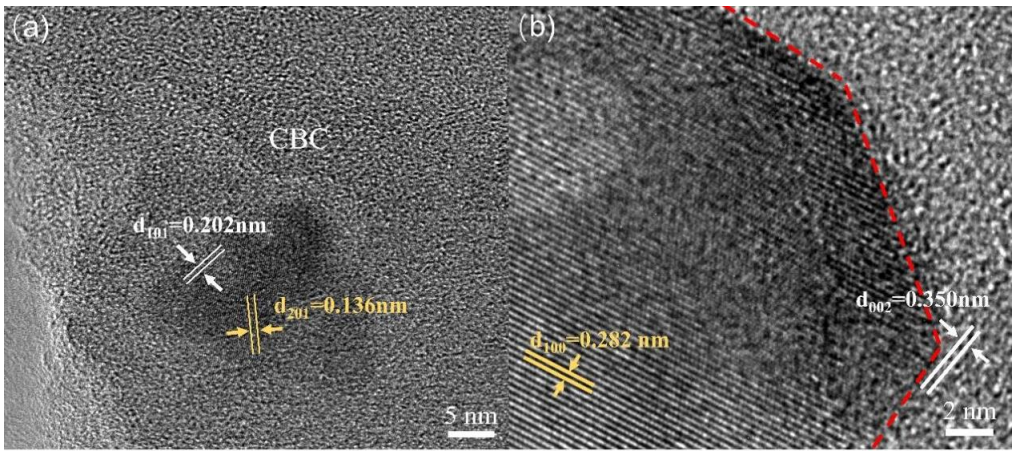

Figure 4. TEM images of ZnO/CBC-60%.

As shown in the Raman spectrum in Figure 5a, it can be observed that peak D and peak G of typical carbon materials were located at 1340 cm^{-1} and 1584 cm^{-1}, respectively, where peak D represents sp^3 hybrid carbon of disordered or defective carbon, while peak G corresponds to sp^2 hybrid carbon of graphite structure [34]. The relative strength ratio (I_D/I_G) of peak D and peak G indicates the degree of graphitization of the material. The I_D/I_G values of pure carbon and ZnO/CBC-60% were 0.90 and 0.79, respectively, which were much higher than the I_D/I_G values of typical graphite, indicating that the prepared carbon materials were not highly crystalline and disordered materials exist. This was consistent with the observation of XRD. Moreover, the addition of ZnO improved the degree of disorder and defects in the structure of carbon materials [35]. The peaks at 80 cm^{-1} and 427 cm^{-1} in ZnO/CBC-60% correspond to E_2^{low} and E_2^{high}, respectively. E_2^{low} was affected by Zn^{2+} gap defect, and E_2^{high} was affected by O^{2-} vacancy [36]. The simultaneous appearance of characteristic peaks of ZnO and carbon materials confirmed the successful preparation of ZnO/CBC. At the same time, it can be observed from Figure 6b that the D-peaks and G-peaks of ZnO/CBC-60% had a certain wave number displacement relative to pure carbon materials. It can be concluded that the heterojunction constructed by ZnO and cellulose-based carbon induces charge transfer between them [17].

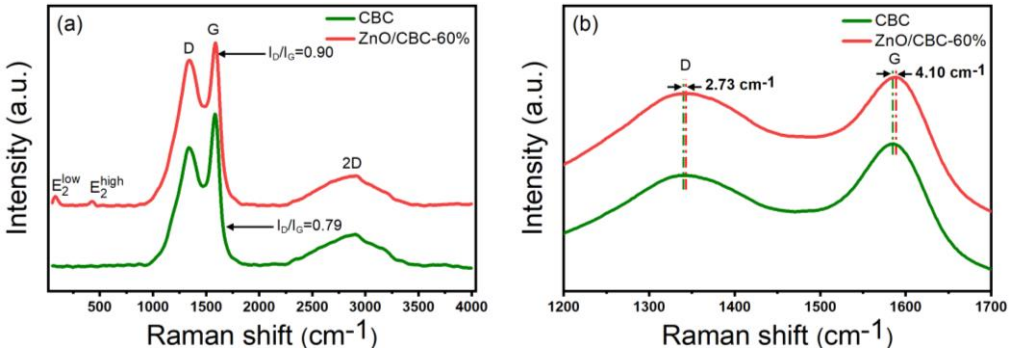

Figure 5. (a) Raman spectra of ZnO/CBC-60% and CBC, (b) Partial enlarged Raman spectra of ZnO/CBC-60% and CBC.

In order to verify the elemental composition and surface chemical information of ZnO/CBC-60%, the materials were characterized by XPS. Figure 6a shows that ZnO/CBC-60% were mainly composed of Zn, C and O elements. Figure 6b was the high-resolution spectrum of Zn^{2p}. In the figure, the peaks of $Zn^{2p1/2}$ and $Zn^{2p3/2}$ were 1044.0 eV and 1021.1 eV respectively, and the binding energy distance before the two peaks was 22.9 eV, which proved the existence of divalent zinc ions[37]. Figure 6c shows the high resolution spectrum of O 1s. O 1s can be deconvolved into three peaks centered on 529.5 eV, 531.2 eV and 532.2 eV. The peak at 529.5 eV is attributed to the O^{2-} ion in the Zn-O bond in the ZnO wurtzite structure, and the peak at 531.2 eV is attributed to the Zn-O-C bond and the

Preprints (www.preprints.org) | NOT PEER-REVIEWED | Posted: 14 November 2023 doi:10.20944/preprints202311.0857.v1

adsorbed hydroxyl group or water. The peak at 532.2 eV is attributed to the carbonate (C-O /C=O) species [38]. As shown in Figure 6d, three peaks appeared at 283.6 eV, 285.7 eV and 288.3 eV respectively, which belonged to the Zn-C bond, Zn-O-C bond and C=O bond respectively, indicating that the performance of ZnO/CBC-60% was different from that of pure ZnO [39].

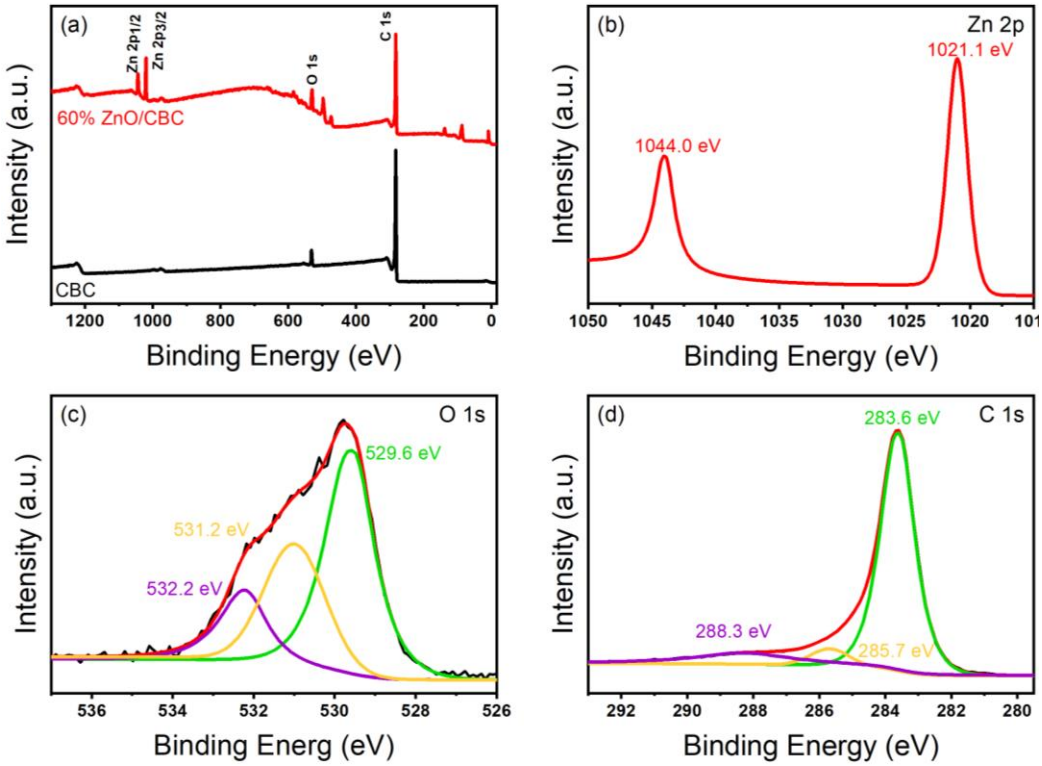

Figure 6. XPS patterns of ZnO/C-60% and CBC. (a) Full spectrum of sample, (b) Zn 2p XPS spectra of ZnO/CBC-60%, (c) C 1s XPS spectra of ZnO/CBC-60%, (d) O 1s XPS spectra of ZnO/CBC-60%.

Mott Schottky curve was used to determine the semiconductor type of the material to better explain the sensing mechanism of the material. Figure S2 shows the Mott Schottky curves of CBC and ZnO/CBC-60% at different frequencies measured at room temperature. It can be seen from the figure that the slopes of all curves are negative, indicating that CBC was a p-type semiconductor, and the prepared ZnO/CBC-60% also exhibited p-type semiconductor properties.

3.2. Results of Sensing Tests

Firstly, the gas sensing response of ZnO/CBC with different contents of CBC and ZnO precursors to 200 ppm ammonia at room temperature of 60% relative humidity was tested. When the sensor was in an air environment, the resistance of the sensor was at a stable value (R_a). When exposed to ammonia, the resistance of the sensor increased and reached a maximum value (R_g). When the sensor is exposed to air again, the resistance of the sensor will gradually return to the initial value (R_a). The resistance of CBC and ZnO/CBC increased gradually in ammonia environment and decreased gradually in air, which showed p-type semiconductor behavior. After testing the sensor, Figure 7a shows that when the ZnO precursor content was 60%, the sensor's gas sensing response to 200 ppm ammonia was the highest, reaching 27%. Therefore, zinc acetate/cellulose (wt%) =150 wt% was selected as the optimal ratio for preparing the required sensing material. At the same time, the ZnO/CBC-60% sensor was placed in the environment of methanol, isopropyl alcohol, ethanol and formaldehyde at 200 ppm at room temperature to test the gas sensing performance of the sensor to these gases, in order to verify the selectivity of the sensor to ammonia. It can be seen from Figure 7b that the gas sensing response of the sensor to ammonia is dozens of times that of other gases, indicating that the prepared ZnO/CBC-60% sensor had good selectivity to ammonia. This may be

Preprints (www.preprints.org) | NOT PEER-REVIEWED | Posted: 14 November 2023 doi:10.20944/preprints202311.0857.v1

attributed to the fact that the heterostructure constructed between ZnO and CBC provided more active sites for the selective adsorption of ammonia molecules.

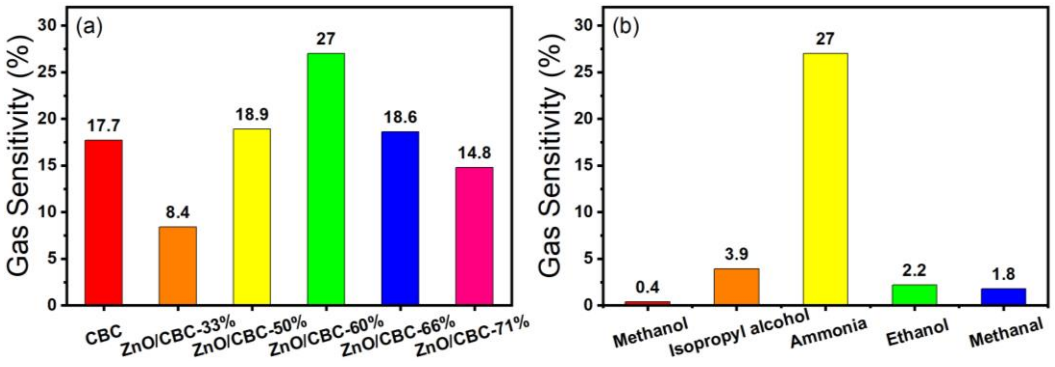

Figure 7. (a) Response of different amounts of zinc oxide and CBC to ammonia at 200 ppm concentration, (b) Selectivity of ZnO/CBC-60% for ammonia.

In order to further test the gas sensing performance of ZnO/CBC-60% for ammonia. Sensor was put in ammonia environment with five concentrations of 25 ppm, 50 ppm, 100 ppm, 150 ppm and 200 ppm at room temperature for gas sensing test. The gas sensing response of the sensor to ammonia with a concentration of 25-200 ppm at room temperature is shown in figure 8a. As the ammonia concentration increased, the gas sensing response of the sensor increased, which was in line with the expected goals of the experiment. Stability is one of the key parameters of gas sensing. We tested the stability of ZnO/CBC-60% sensor by placing the sensor in 200 ppm ammonia environment for five rounds of gas sensing tests. As shown in figure 8b, after five sensing cycled, the gas sensing performance of ZnO/CBC-60% sensor had not weakened, indicating that the sensor had good repeatability.

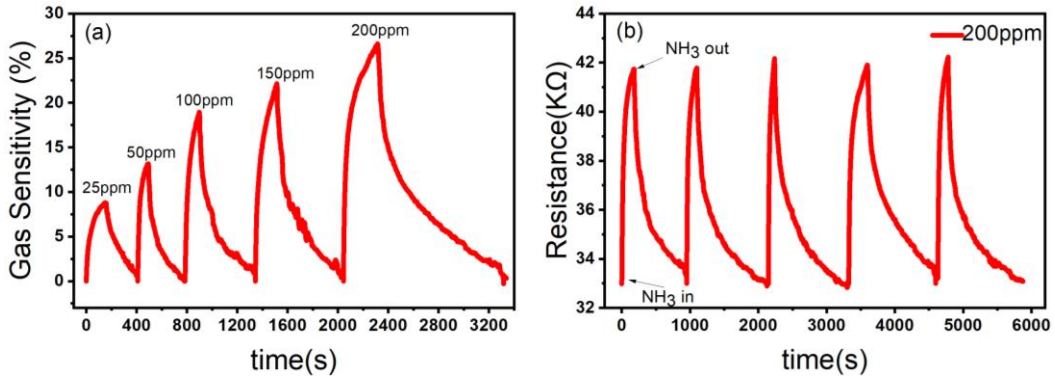

Figure 8. (a) Response of ZnO/CBC-60% to ammonia with concentration of 25-200 ppm, (b) Repeatability evaluation of ZnO/CBC-60% for 200 ppm ammonia at RT.

Relative humidity is an important factor affecting the performance of gas sensor [40]. as shown in Figure 9a, with the increase of relative humidity, the gas sensitivity of ZnO/CBC-60% sensor to ammonia was correspondingly weakened, which may be due to the fact that H_2O molecules in the test environment preempted the active sites, so that NH_3 molecules could not fully react with the materials, resulting in the decrease of gas sensing response[18].

The ZnO/CBC-60% sensor was put in an ammonia concentration environment of 200 ppm for one week. As can be seen from Figure 9b, the gas sensing response of the sensor to ammonia had not changed greatly, which indicated that the sensor had good stability.

Preprints (www.preprints.org) | NOT PEER-REVIEWED | Posted: 14 November 2023 doi:10.20944/preprints202311.0857.v1

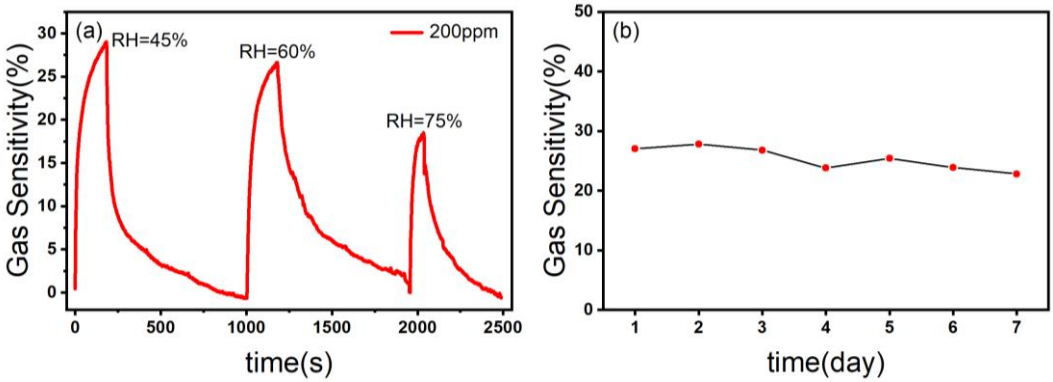

Figure 9. (a) The response curves of ZnO/CBC-60% towards 200 ppm ammonia at different RHs, (b) Stability test of ZnO/CBC-60% for 200 ppm ammonia within one week at RT.

4. Discussion

In order to prove that the gas sensing response of ZnO/CBC-60% was the result of the reaction with NH_3 molecules, the material was analyzed by in-situ DRIFT spectroscopy. As shown in Figure 10a, after introducing the mixed gas of NH_3 and N_2, it can be observed that adsorption peaks of coordinated NH_3 species corresponding to Lewis sites appeared near 929, 964, 1619 and 3334 cm^{-1} [41–43], and these peaks gradually became stronger with the increase of adsorption time. Figure 10b shows that the peak value was obviously weakened after N_2 purging. These phenomena show that the adsorption and desorption of ammonia occurred on the surface of ZnO/CBC-60%, which explained the gas sensing response of ZnO/CBC-60% to ammonia.

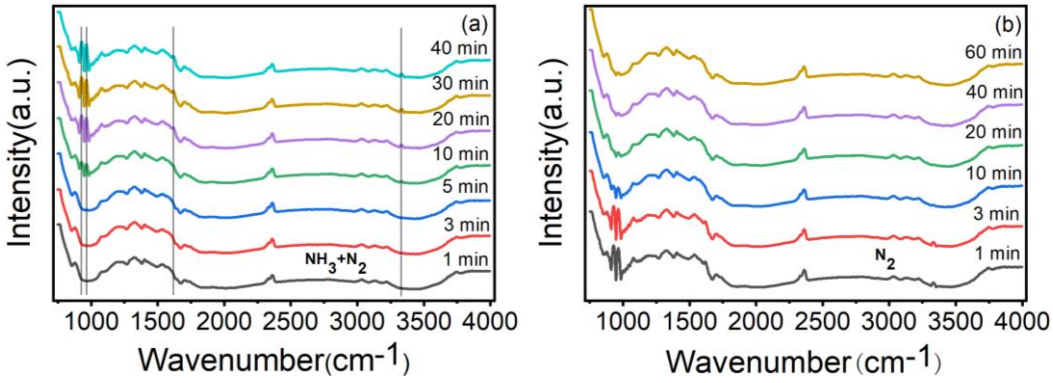

Figure 10. (a) In-situ DRIFT spectroscopy of ZnO/CBC-60% by passing NH_3+N_2 mixture gases at RT for 40 mins, (b) Purged by N_2 at RT.

Figure 11 shows the interface energy band diagram of ZnO/CBC sensor in air and ammonia. It can be seen from Mott Schottky curve that CBC was a p-type semiconductor, while ZnO was a typical n-type semiconductor, The combination of the two created a p-n heterojunction. Due to the difference in concentration of electrons and holes in the two materials, the free electrons ZnO conduction band will diffuse to CBC, and the holes in CBC will diffuse to ZnO until the Fermi level reached a new equilibrium [44,45]. This process made the energy band bend, forming a narrow depletion layer, forming an electron accumulation layer on the CBC side and a hole accumulation layer on the ZnO side. When ZnO/CBC sensor was exposed to ammonia, NH_3 molecules will capture hole protons from CBC, and the hole accumulation layer will provide more adsorption sites for ammonia adsorption. In addition, NH_3 molecules will release some electrons to ZnO/CBC, which will neutralize the holes and further widen the depletion layer on the CBC side, resulting in an obvious increase [46], in the resistance of the sensor, which was consistent with the phenomenon in gas sensing test.

Preprints (www.preprints.org) | NOT PEER-REVIEWED | Posted: 14 November 2023 doi:10.20944/preprints202311.0857.v1

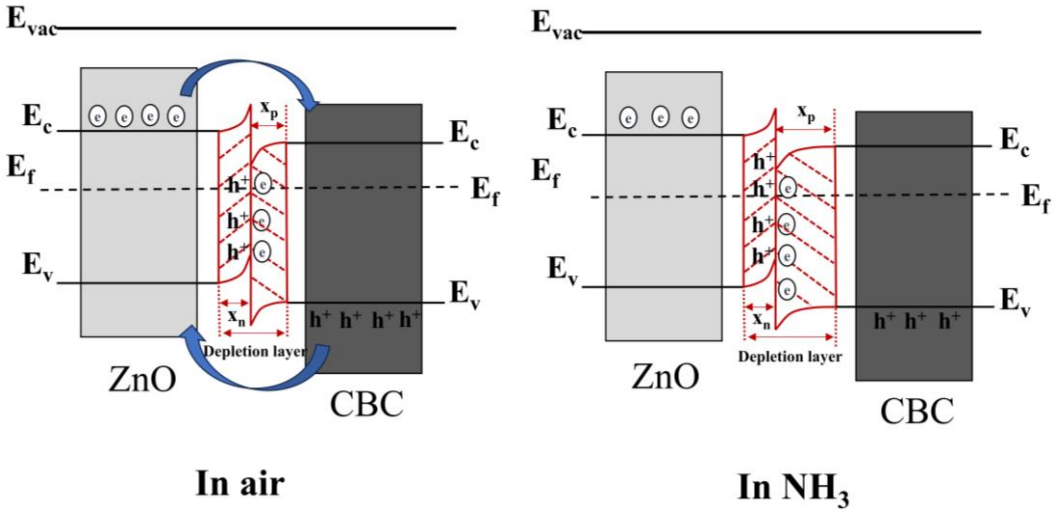

Figure 11. The energy band structure diagram of n-type ZnO/p-type CBC hetero-contact.

5. Conclusions

In this experiment, ZnO was loaded on CBC, and the gas sensing response of ZnO/CBC loaded with different ZnO contents to ammonia at room temperature was studied by various the content of ZnO precursors. The composites were characterized by SEM, TEM, XRD, Raman and XPS. The results showed that ZnO had been successfully loaded on CBC. Subsequently, the gas sensing performance showed that the ZnO/CBC with 60% ZnO precursor content had better gas sensing response to 200 ppm ammonia at room temperature, reaching 27%. In addition, through five consecutive rounds of gas sensing response tests in 200 ppm ammonia environment, it was found that ZnO/CBC-60% exhibited good stability. At the same time, by comparing the gas sensing performance of several VOC gases, it was found that the material for ammonia had well selectivity. In-situ DRIFT spectroscopy proved that the sensing material did react with ammonia, and the ZnO/CBC-60% could provide more active sites for ammonia molecules because of the construction of heterojunction between ZnO and CBC. Therefore, ZnO/CBC composites had improved sensing performance. This study provides a new idea for the design and synthesis of biomass carbon-metal oxide composites.

Supplementary Materials: The following supporting information can be downloaded at the website of this paper posted on Preprints.org, Figure S1: (a-e) SEM images of the ZnO/CBC-60% and corresponding mapping images of C, O and Zn, (f) the EDS analysis of the prepared ZnO/CBC-60%; Figure S2: Figure S2. Mott-Schottky curves of (a) CBC, (b) ZnO/CBC-60%.

Author Contributions: Conceptualization, H.X., X.-P.L. and Y.-X.W.; methodology, H.X. and Z.-X.G.; software, H.X. C. G.; validation, H.X. and Z.-X.G.; formal analysis, L.-Z.H.; investigation, H.X.; resources, H.X., X.-P.L and Y.-X.W.; data curation, H.X. and Z.-X.G.; writing—original draft preparation, X.H.; writing—review and editing, H.X., X.-J.Y., X.-P.L. and Y.-X.W.; visualization, H.X.; supervision, L.-Z.H.; project administration, H.X., Y.-X.W. and X.-P.L; funding acquisition, X.-P.L. All authors have read and agreed to the published version of the manuscript.

Funding: This research was funded by the Central Financial Funds for the Forestry Science and Technology Promotion Application Project in China (2023TS01), Zhejiang A & F University Scientific Research and Development Fund Project grant number (2020RC032), the "Pioneer" and "Leading Goose" R&D Program of Zhejiang (2022C02023).

Data Availability Statement: The data presented in this study are available on request from the corresponding author.

Conflicts of Interest: The authors declare no conflict of interest.

Preprints (www.preprints.org) | NOT PEER-REVIEWED | Posted: 14 November 2023 doi:10.20944/preprints202311.0857.v1

References

1. Danasa, A.S.; Soesilo, T.E.B.; Martono, D. N.; Sodri, A.; Hadi, A.S.; Chandrasa, G.T. *The ammonia release hazard and risk assessment: A case study of urea fertilizer industry in Indonesia. IOP conference series: Earth and environmental science, 2019;* IOP Publishing: 2019; pp. 012087. DOI 10.1088/1755-1315/399/1/012087
2. Aarya, S.; Kumar, Y.; Chahota, R. K. Recent Advances in Materials, Parameters, Performance and Technology in Ammonia Sensors: A Review. *J. Inorg. Organomet. Polym Mater.* **2020,** *30 (2),* 269-290. DOI 10.1007/s10904-019-01208-x
3. Si, X.; Wei, Y.; Wang, C.; Li, L.; Ding, Y. A sensitive electrochemical sensor for ofloxacin based on a graphene/zinc oxide composite film. *Anal. Methods* **2018,** *10 (17),* 1961-1967. DOI 10.1039/C8AY00127H
4. Dai, H.; Feng, N.; Li, J.; Zhang, J.; Li, W. Chemiresistive humidity sensor based on chitosan/zinc oxide/single-walled carbon nanotube composite film. *Sensor Acturt B-Chem* **2019,** *283,* 786-792. DOI 10.1016/j.snb.2018.12.056
5. Young, S.J.; Liu, Y.H.; Shiblee, M. N. I.; Ahmed, K.; Lai, L.T.; Nagahara, L.; Thundat, T.; Yoshida, T.; Arya, S.;Furukawa, H. Flexible ultraviolet photodetectors based on one-dimensional gallium-doped zinc oxide nanostructures. *ACS Appl. Electron. Mater* **2020,** *2 (11),* 3522-3529. DOI 10.1021/acsaelm.0c00556
6. Yu, S.; Chen, C.; Zhang, H.; Zhang, J.; Liu, J. Design of high sensitivity graphite carbon nitride/zinc oxide humidity sensor for breath detection. *Sensor Acturt B-Chem* **2021,** *332,* 129536. DOI 10.1016/j.snb.2021.129536
7. Chauhan, R.; Kumar, A.; Tripathi, R.; Kumar, A. Advancing of zinc oxide nanoparticles for cosmetic applications. In *Handbook of consumer Nanoproducts,* Springer: Singapore, 2022; pp. 1-16. DOI 10.1007/978-981-15-6453-6_100-1
8. Kanaparthi, S.; Singh, S. G. Chemiresistive sensor based on zinc oxide nanoflakes for CO_2 detection. *ACS Appl. Nano Mater* **2019,** *2 (2),* 700-706. DOI 10.1021/acsanm.8b01763
9. Zhang, Y.; Liu, T.; Hao, J.; Lin, L.; Zeng, W.; Peng, X.; Wang, Z. Enhancement of NH_3 sensing performance in flower-like ZnO nanostructures and their growth mechanism. *Appl. Surf. Sci* **2015,** *357,* 31-36. DOI 10.1016/j.apsusc.2015.08.170
10. Ganesh, R. S.; Durgadevi, E.; Navaneethan, M.; Patil, V.; Ponnusamy, S.; Muthamizhchelvan, C.; Kawasaki, S.; Patil, P.; Hayakawa, Y. Tuning the selectivity of NH_3 gas sensing response using Cu-doped ZnO nanostructures. *Sensor Actuat A: Phy* **2018,** *269,* 331-341. DOI 10.1016/j.sna.2017.11.042
11. Poloju, M.; Jayababu, N.; Reddy, M. R. Improved gas sensing performance of Al doped ZnO/CuO nanocomposite based ammonia gas sensor. *Mater Sci Eng B-Adv* **2018,** *227,* 61-67. DOI 10.1016/j.mseb.2017.10.012
12. Zhao, Z.; Yang, H.; Wei, Z.; Xue, Y.; Sun, Y.; Zhang, W.; Li, P.; Gong, W.; Zhuiykov, S.; Hu, J. NH_3 sensor based on 3D hierarchical flower-shaped n-ZnO/p-NiO heterostructures yields outstanding sensing capabilities at ppb level. *Sensors-Basel* **2020,** *20 (17),* 4754. DOI 10.3390/s20174754
13. Abdulsattar, M. A.; Jabbar, R. H.; Abed, H. H.; Abduljalil, H. M. The sensitivity of pristine and Pt doped ZnO nanoclusters to NH_3 gas: A transition state theory study. *Optik* **2021,** *242,* 167158. DOI 10.1016/j.ijleo.2021.167158
14. Ramesh, A.; Gavaskar, D.; Nagaraju, P.; Duvvuri, S.; Vanjari, S. R. K.; Subrahmanyam, C. Mn-doped ZnO microspheres prepared by solution combustion synthesis for room temperature NH_3 sensing. *Appl. Surf. Sci.Adv* **2022,** *12,* 100349. DOI 10.1016/j.apsadv.2022.100349
15. Chao, J.; Chen, Y.; Xing, S.; Zhang, D.; Shen, W. Facile fabrication of ZnO/C nanoporous fibers and ZnO hollow spheres for high performance gas sensor. *Sensor Acturt B-Chem* **2019,** *298,* 126927. DOI 10.1016/j.snb.2019.126927
16. Sun, Q.; Wu, Z.; Zhang, M.; Qin, Z.; Cao, S.; Zhong, F.; Li, S.; Duan, H. M.; Zhang, J. Improved Gas-Sensitive Properties by a Heterojunction of Hollow Porous Carbon Microtubes Derived from Sycamore Fibers. *ACS Sustainable Chem. Eng* **2021,** *43,* 9. DOI 10.1021/acssuschemeng.1c02956
17. Hu, J.; Yin, C.; Cheng, M.; Wei, T.; Liu, Q.; Li, W.; Ling, Y.; Zhang, Y.; Liu, B. Facile synthesis of N-doped carbon sheets-ZnO hybrids for NO2 sensing at ppb level. *J. Alloys Compd* **2022,** *892,* 162243. DOI 10.1016/j.jallcom.2021.162243
18. Tu, H.; Zhu, M.; Duan, B.; Zhang, L. Recent progress in high-strength and robust regenerated cellulose materials. *Adv. Mater* **2021,** *33 (28),* 2000682. DOI 10.1002/adma.202000682
19. Shao, H.; Wu, Y.-C.; Lin, Z.; Taberna, P.-L.; Simon, P. Nanoporous carbon for electrochemical capacitive energy storage. *Chem. Soc. Rev* **2020,** *49 (10),* 3005-3039. DOI 10.1039/D0CS00059K
20. Gan, L.; Geng, A.; Song, C.; Xu, L.; Wang, L.; Fang, X.; Han, S.; Cui, J.; Mei, C. Simultaneous removal of rhodamine B and Cr (VI) from water using cellulose carbon nanofiber incorporated with bismuth oxybromide: The effect of cellulose pyrolysis temperature on photocatalytic performance. *Environ. Res* **2020,** *185,* 109414. DOI 10.1016/j.envres.2020.109414
21. Dou, T.; Zang, L.; Zhang, Y.; Sun, Z.; Sun, L.; Wang, C. Hybrid g-C_3N_4 nanosheet/carbon paper membranes for the photocatalytic degradation of methylene blue. *Mater. Lett* **2019,** *244,* 151-154. DOI 10.1016/j.matlet.2019.02.066

Preprints (www.preprints.org) | NOT PEER-REVIEWED | Posted: 14 November 2023 doi:10.20944/preprints202311.0857.v1

22. Habibi, S.; Jamshidi, M. Sol–gel synthesis of carbon-doped TiO_2 nanoparticles based on microcrystalline cellulose for efficient photocatalytic degradation of methylene blue under visible light. *Environ. Technol* **2019,** *41 (24),* 3233-3247. DOI 10.1080/09593330.2019.1604815
23. Gan, L.; Geng, A.; Xu, L.; Chen, M.; Wang, L.; Liu, J.; Han, S.; Mei, C.; Zhong, Q. The fabrication of bio-renewable and recyclable cellulose based carbon microspheres incorporated by $CoFe_2O_4$ and the photocatalytic properties. *J. Cleaner Prod* **2018,** *196,* 594-603. DOI 10.1016/j.jclepro.2018.06.086
24. John, R. A. B.; Shruthi, J.; Reddy, M. R.; Kumar, A. R. Manganese doped nickel oxide as room temperature gas sensor for formaldehyde detection. *Ceram. Int* **2022,** *48 (12),* 17654-17667. DOI 10.1016/j.ceramint.2022.03.036.
25. Chen, Q.; Ma, S.; Xu, X.; Jiao, H.; Zhang, G.; Liu, L.; Wang, P.; Gengzang, D.; Yao, H. Optimization ethanol detection performance manifested by gas sensor based on In_2O_3/ZnS rough microspheres. *Sensor Acturt B-Chem* **2018,** *264,* 263-278. DOI 10.1016/j.snb.2018.02.172
26. Mohan, S.; Vellakkat, M.; Aravind, A.; Reka, U. Hydrothermal synthesis and characterization of Zinc Oxide nanoparticles of various shapes under different reaction conditions. *Nano Express* **2020,** *1 (3),* 030028. DOI 10.1088/2632-959X/abc813
27. Bagheri, F.; Haratizadeh, H. UV-activated CO_2 sensor based on ZnO nanoparticles at low temperatures. *Mater. Sci. Semicond. Process* **2022,** *141,* 106422. DOI 10.1016/j.mssp.2021.106422
28. Liu, Y.; Lu, Y. X.; Xu, Y. S.; Meng, Q. S.; Gao, J. C.; Sun, Y. G.; Hu, Y. S.; Chang, B. B.; Liu, C. T.; Cao, A. M. Pitch-derived soft carbon as stable anode material for potassium ion batteries. *Adv. Mater* **2020,** *32 (17),* 2000505. DOI 10.1002/adma.202000505
29. Li, K.; Liu, Q.; Cheng, H.; Hu, M.; Zhang, S. Classification and carbon structural transformation from anthracite to natural coaly graphite by XRD, Raman spectroscopy, and HRTEM. *Spectrochim Acta A* **2021,** *249,* 119286. DOI 10.1016/j.saa.2020.119286
30. Dong, Y.; Zhu, X.; Pan, F.; Deng, B.; Liu, Z.; Zhang, X.; Huang, C.; Xiang, Z.; Lu, W. Mace-like carbon fiber/ZnO nanorod composite derived from Typha orientalis for lightweight and high-efficient electromagnetic wave absorber. *Adv. Compos. Hybrid Mater* **2021,** *4 (4),* 1002-1014. DOI 10.1007/s42114-021-00277-2
31. Xu, H.; Wang, H.; Zhang, Y.; He, W.; Zhu, M.; Wang, B.; Yan, H., Hydrothermal synthesis of zinc oxide powders with controllable morphology. *Ceram Int* **2004,** *30 (1),* 93-97. DOI 10.1016/S0272-8842(03)00069-5
32. Chang, X.; Li, K.; Qiao, X.; Xiong, Y.; Xia, F.; Xue, Q. ZIF-8 derived ZnO polyhedrons decorated with biomass derived nitrogen-doped porous carbon for enhanced acetone sensing. *Sensor Actuat B: Chem* **2021,** *330,* 129366. DOI 10.1016/j.snb.2020.129366
33. Chen, J.; Lv, H.; Bai, X.; Liu, Z.; He, L.; Wang, J.; Zhang, Y.; Sun, B.; Kan, K.; Shi, K. Synthesis of hierarchically porous Co_3O_4/Biomass carbon composites derived from MOFs and their highly NO_2 gas sensing performance. *Microporous Mesoporous Mater* **2021,** *321,* 111108. DOI 10.1016/j.micromeso.2021.111108
34. Qin, Z.; Wu, Z.; Sun, Q.; Sun, J.; Zhang, M.; Shaymurat, T.; Lv, C.; Duan, H., Biomimetic gas sensor derived from disposable bamboo chopsticks for highly sensitive and selective detection of NH_3. *Chem. Eng. J* **2023,** *462,* 142203. DOI 10.1016/j.cej.2023.142203
35. Nada, A. A.; Orimolade, B. O.; El-Maghrabi, H. H.; Koiki, B. A.; Rivallin, M.; Bekheet, M. F.; Viter, R.; Damberga, D.; Lesage, G.; Iatsunskyi, I. Photoelectrocatalysis of paracetamol on Pd–ZnO/N-doped carbon nanofibers electrode. *Appl. Mater. Today* **2021,** *24,* 101129. DOI 10.1016/j.apmt.2021.101129
36. e Silva, R. L. d. S.; Franco Jr, A. Raman spectroscopy study of structural disorder degree of ZnO ceramics. *Mater. Sci. Semicond. Process* **2020,** *119,* 105227. DOI 10.1016/j.mssp.2020.105227
37. Hussain, M. Z.; Pawar, G. S.; Huang, Z.; Tahir, A. A.; Fischer, R. A.; Zhu, Y.; Xia, Y. Porous ZnO/Carbon nanocomposites derived from metal organic frameworks for highly efficient photocatalytic applications: A correlational study. *Carbon* **2019,** *146,* 348-363. DOI 10.1016/j.carbon.2019.02.013
38. Hu, C.; Hu, X.; Li, R.; Xing, Y. MOF derived ZnO/C nanocomposite with enhanced adsorption capacity and photocatalytic performance under sunlight. *J. Hazard. Mater* **2020,** *385,* 121599. DOI 10.1016/j.jhazmat.2019.121599
39. Zhang, H.; Pan, Q.; Cai, W.; Shi, X.; Yang, D.-P.; Lin, H.; Qiu, E. C-doped ZnO Nanocomposites Molecularly Imprinted Photoelectrochemical Sensor for Ultrasensitive and Selective Detection of Oxytetracycline in Milk. *Food Chem* **2023,** *426,* 136535. DOI 10.1016/j.foodchem.2023.136535
40. Liu, C.; Duan, Z.; Zhang, B.; Zhao, Y.; Yuan, Z.; Zhang, Y.; Wu, Y.; Jiang, Y.; Tai, H. Local Gaussian process regression with small sample data for temperature and humidity compensation of polyaniline-cerium dioxide NH_3 sensor. *Sensor Actuat B: Chem* **2023,** *378,* 133113. DOI 10.1016/j.snb.2022.133113
41. Fu, Y.; Wang, T.; Wang, X.; Li, X.; Zhao, Y.; Li, F.; Zhao, G.; Xu, X. Investigation of pn sensing transition and related highly sensitive NH_3 gas sensing behavior of SnP_x/rGO composites. *Chem. Eng. J* **2023,** *471,* 144499. DOI 10.1016/j.cej.2023.144499

Preprints (www.preprints.org) | NOT PEER-REVIEWED | Posted: 14 November 2023 doi:10.20944/preprints202311.0857.v1

42. Li, Q.; Hou, Y.; Wang, J.; Liu, Y.; Xiang, N.; Huang, Z. Superiority of raw biomass and potassium hydroxide in preparation of ultrahigh nitrogen doping of carbon for NH_3-SCR reaction. *ACS Sustainable Chem. Eng* **2020,** *8 (30),* 11308-11316. DOI 10.1021/acssuschemeng.0c03193
43. Wang, J.; Yan, Z.; Liu, L.; Zhang, Y.; Zhang, Z.; Wang, X. Low-temperature SCR of NO with NH_3 over activated semi-coke composite-supported rare earth oxides. *Appl. Surf. Sci* **2014,** *309,* 1-10. DOI 10.1016/j.apsusc.2014.04.112
44. Liu, J.; Zhu, B.; Zhang, L.; Fan, J.; Yu, J. 0D/2D CdS/ZnO composite with nn heterojunction for efficient detection of triethylamine. *J. Colloid Interface Sci* **2021,** *600,* 898-909. DOI 10.1016/j.jcis.2021.05.082
45. Qin, S.; Tang, P.; Feng, Y.; Li, D. Novel ultrathin mesoporous ZnO-SnO_2 nn heterojunction nanosheets with high sensitivity to ethanol. *Sensor Actuat B: Chem* **2020,** *309,* 127801. DOI 10.1016/j.snb.2020.127801
46. Tian, X.; Cui, X.; Xiao, Y.; Chen, T.; Xiao, X.; Wang, Y. Pt/MoS_2/Polyaniline Nanocomposite as a Highly Effective Room Temperature Flexible Gas Sensor for Ammonia Detection. *ACS Appl. Mater. Interfaces* **2023,** *15 (7),* 9604-9617. DOI 10.1021/acsami.2c20299

Disclaimer/Publisher's Note: The statements, opinions and data contained in all publications are solely those of the individual author(s) and contributor(s) and not of MDPI and/or the editor(s). MDPI and/or the editor(s) disclaim responsibility for any injury to people or property resulting from any ideas, methods, instructions or products referred to in the content.